Two different mechanisms of stabilization of regular π-stacks of radicals in switchable dithiazolyl-based materials

Tommaso Francese[a,b,‡], Sergi Vela[c], Mercè Deumal[a], Fernando Mota[a], Juan J. Novoa[a], Matteo Farnesi Camellone[d], Stefano Fabris[d], Remco W.A. Havenith[b,e], Ria Broer[b], Jordi Ribas-Arino[a,*]

[a] *Departament de Ciència dels Materials i Química Física and IQTCUB, Universitat de Barcelona, Martí i Franquès 1, Barcelona, E-08028, Spain*.

[b] *Theoretical Chemistry, Zernike Institute for Advance Materials, University of Groningen, Nijenborgh 4, 9747 AG Groningen, The Netherlands*

[c] *Laboratory for Computational Molecular Design, Institute of Chemical Sciences and Engineering, EPFL, CH- 1015 Lausanne, Switzerland*

[d] *CNR-IOM, Consiglio Nazionale delle Ricerche–Istituto Officina dei Materiali, c/o SISSA, via Bonomea 265, 34136 Trieste, Italy*

[e] *Stratingh Institute for Chemistry, University of Groningen, 9747 AG Groningen, The Netherlands*

‡ *Present address: Pritzker School of Molecular Engineering, The University of Chicago, Eckhardt Research Center 5640 S. Ellis Ave. ACC 205, Chicago, IL, USA*

* j.ribas@ub.edu

Abstract

Materials based on regular π-stacks of planar organic radicals are intensively pursued by virtue of their technologically relevant properties. Yet, these π-stacks are commonly unstable against π-dimerization. In this computational study, we reveal that regular π-stacks of planar dithiazolyl radicals can be rendered stable, in some range of temperatures, via two different mechanisms. When the radicals of a π-stack are both longitudinally and latitudinally slipped with respect to each other, the corresponding regular π-stacked configuration is associated with a locally stable minimum in the potential energy surface of the system. Conversely, those regular π-stacks in which radicals are latitudinally slipped with respect to each other are stable as a result of a dynamic interconversion between two degenerate dimerized configurations. The existence of two stabilization mechanisms, which can be traced back to the bonding properties of isolated π-dimers, translates into two different ways of exploiting spin-Peierls-like transitions in switchable dithiazolyl-based materials.

Introduction

π-Stacking is a very common structural motif[1] in materials based on stable planar organic radicals.[2,3,4,5,6] These crystal packing architectures have been extensively pursued and investigated for many years because they can endow materials with interesting magnetic[7,8], conducting[9,10,11,12] and optical properties.[13,14] The numerous examples of planar organic radicals (neutral and charged) exhibiting π-stacks in the solid state include tetrathiafulvalenes[10,15], tetracyanoquinodimethanes[16], tetrathiobenzenes[17], semiquinones[18,19], verdazyls[20,21], phenalenyls[22,23], benzotriazinyls[24,25], metal bis(1,2-dithiolene) complexes[26,27], dithiadiazolyls[28,29,30,31], 1,3,2-dithiazolyls[32,33,34], and bis-1,2,3-dithiazolyls[35,36,37,38]. Some of these radicals can arrange as regular columns with a uniform intermolecular spacing $(\cdots A\cdots A\cdots A\cdots)_n$, or as distorted columns with alternating long and short intermolecular contacts along the π-stacking direction $(\cdots A–A\cdots A–A\cdots)_n$. The latter distorted or dimerized patterns are intrinsically more stable than the regular ones by virtue of the formation of long, multicenter bonds[39,40] (alternatively called "pancake" bonds[41,42,43]) between those radicals that have close contacts (i.e. those radicals forming a π-dimer). Notwithstanding the greater stability of the dimerized π-stacks, their associated physical properties are usually much less appealing than those of regular π-stacks: while regular motifs can give rise to (semi)conducting and/or magnetic materials, distorted arrangements usually lead to diamagnetic and insulating (or weakly semiconductor) materials. It then follows that regular π-stacks are the technologically relevant structural motifs. For this reason, developing a detailed understanding of the mechanisms that render regular π-stacks stable by suppressing π-dimerization is of paramount importance for the design of materials based on π-stacked architectures of organic radicals.

Some specific organic-radical-based crystals present two different polymorphs – a low-temperature (LT) polymorph comprised of dimerized π-stacks and a high-temperature (HT) polymorph comprised of regular π-stacks – that can be interconverted between each other by means of temperature changes[33,34,44,45,46,47,48,49] and even by photoirradiation[50]. Therefore, π-stacks of planar organic

radicals can also be harnessed for the development of dynamic molecular crystals whose physical properties can be switched by external stimuli.[51,52] In these cases, a detailed knowledge of the underlying mechanism of the stability of regular π-stacks can be also beneficial for tailoring the phase transition temperature by means of crystal engineering. Here, we will investigate by computational means the structural properties of the uniform stacks of two switchable materials belonging to the family of 1,3,2-dithiazolyls.

The crystals of the 1,3,2-dithiazolo[4,5-b]pyrazin-2-yl[45] (PDTA, **1**) and 1,2,5-thiadiazolo[3,4-b]-1,3,2-dithiazolo[3,4-b]pyrazin-2-yl[44] (TDPDTA, **2**) radicals undergo hysteretic phase transitions between two polymorphs with different magnetic properties. As a result, these two crystals have become notable examples of magnetic bistability, a technologically relevant property that is sought-after[53,54] due to the memory effect intrinsically associated with a hysteresis loop.[55] Other organic radicals exhibiting magnetic bistability include additional 1,3,2-dithiazolyls[33,56], bis-1,2,3-dithiazolyls[57,58], nitroxides[59], spirobiphenalenyls[60,61], and dithiadiazolyls.[62,63] The hysteresis loop of **1** is centered around 323 K and spans 46 K (see Figure 1, right). The different magnetic response of its two polymorphs (LT features diamagnetism, while HT features a weak paramagnetism[45]) results from changes in the antiferromagnetic interactions between adjacent radicals along the π-stacks.[64] The hysteresis loop of **2**, in turn, is centered around 140 K and spans *ca*. 120 K (see Figure 1, left). The two polymorphs of **2** exhibit a weak paramagnetism, the magnetic response of LT being weaker than that of HT. The two different magnetic behaviors are also due to changes in the antiferromagnetic interactions between adjacent radicals along the π-stacks in going from stacks of π-dimerized radicals in LT to regular π-stacks of radicals in HT.[64]

The computational investigation of the structural properties of the π-stacks of **1** and **2** herein presented will bring to light two different mechanisms by which regular π-stacks are rendered stable in the family of planar DTA radicals. We will also demonstrate that the existence of these two mechanisms, which can lead to two different ways of exploiting spin-Peierls-like transitions in switchable dithiazolyl-based materials, arises from the topological features exhibited by the

energy landscape of isolated π-stacking dimers as a function of slippage degrees of freedom.

Results and Discussion

1. Comparison of the X-ray crystal packing of the LT and HT polymorphs of PDTA and TDPDTA

We first compare the crystal packing of the LT and HT polymorphs of PDTA (**1**) and TDPDTA (**2**), whose X-ray data was previously reported[44,45], to stress the similarities and differences presented by their regular and distorted π-stacks of radicals. These stacks can be characterized using three geometrical variables (see Figures 2 and 3), namely, d_{IP}, d_{SL} and d_{LG}, which measure the interplanar distance between adjacent radicals, the degree of latitudinal slippage between adjacent radicals, and the degree of longitudinal slippage, respectively.

The two polymorphs of **1** belong to different space groups (the HT phase is monoclinic, while the LT phase is triclinic) and their crystal structures show some differences (see Figure 2 and Figure S1). While the LT phase presents distorted π-stacks that consist of slipped pairs of nearly eclipsed radicals, the columns of the HT phase are regular π-stacks of radicals, where each molecule exhibits a slipped overlap with its two adjacent molecules along the stacking direction. As can be seen in Figure 2b, the slippage observed in HT is mainly a slippage with respect to the symmetry plane that is perpendicular to the molecular plane (latitudinal slippage, d_{SL}). The LT and HT polymorphs are also different regarding the molecular-plane orientations of PDTA radicals: the molecules in LT are all arranged in parallel planes, whereas HT includes two distinct molecular-plane orientations (see Figure S1).

Regarding the crystal structures of **2**, its two polymorphs belong to the same triclinic space group and they present one single molecular plane orientation (see Figure S2). The columns of the LT polymorph are distorted π-stacks that present

an alternation between shorter and longer intermolecular contacts between adjacent radicals. In the HT polymorph, in turn, radicals pile up on top of each other giving rise to regular π-stacks (see Figure 3). In contrast with **1**, the radicals of **2** present two different types of slippage with respect to their adjacent neighbors along the regular π-stack. Besides the latitudinal slippage (d_{SL}), which is also present in **1**, they show an additional slippage along an orthogonal direction (longitudinal slippage, d_{LG}, see Figure 3).

The cofacial π-dimers in the LT polymorphs of **1** and **2** also show a significant difference between them: while the π-dimers of **1** are nearly eclipsed, there is a notable degree of latitudinal slippage in the π-dimers of **2** (compare Figures 2a and 3a).

2. Minimum energy configurations of the LT and HT polymorphs of PDTA and TDPDTA

Variable-cell geometry optimizations of **1** and **2** were done with the goal of establishing whether the X-ray recorded structures of their LT and HT polymorphs are minimum energy structures on the potential energy surface of the crystals. The model systems for both **1** and **2** were supercells containing 32 DTA radicals, arranged in 8 stacks of 4 radicals each (see Figures S3 and S4). These supercells ensure a representation on an equal footing of both LT and HT polymorphs. The optimized geometries of the LT and HT phases are hereafter referred to as LT-0 and HT-0, respectively.

The results obtained from the optimizations of the LT phases of **1** and **2** show, as expected, that the π-dimers observed in the X-ray structures are preserved in the LT-0 polymorphs. It is also important to stress that the optimized and experimental structures match very well (see Figures S5 and S6). Conversely, the results obtained from the optimizations of the HT polymorphs are more intricate. In the case of **1**, the optimization of its HT phase (**1**-HT) led to an intra-stack dimerization process, as a result of which the uniform separation between

adjacent radicals observed in the X-ray structure was disrupted (see Figures 4a and 4b). Despite this dimerization, the overall monoclinic symmetry of the crystal was preserved throughout the optimization and, therefore, the HT-0 structure of **1** (**1**-HT-0) differs from its LT-0 structure (**1**-LT-0). Note that **1**-LT-0 and **1**-HT-0 contain one and two distinct molecular planes, respectively. It then follows that **1**-HT-0 should in fact be recognized as the low-temperature crystal structure of the HT polymorph of **1**, not yet detected experimentally. The higher stability of **1**-LT-0 compared to **1**-HT-0 (the computed cohesive energies per PDTA radical for the **1**-LT-0 and **1**-HT-0 polymorphs are 24.1 and 23.3 kcal mol^{-1}, respectively) explains why the former is the experimentally observed polymorph in the low-temperature regime. It is noted that the results obtained for **1** are completely analogous to the results previously reported for the 1,3,5-trithia-2,4,6-triazapentalenyl (TTTA) radical.[65] The regular π-stacks of the HT phase of 4-NCBDTA were also found not to be a minimum energy structure at 0 K.[66]

In contrast to the results obtained for **1**-HT, the variable-cell optimization of **2**-HT did not lead to any intra-stack dimerization process. Accordingly, the **2**-HT-0 structure preserves the uniform π-stacking motif observed in the X-ray structure of **2**-HT. In fact, the structure of the columns in **2**-HT-0 and in **2**-HT-293 (*i.e.*, the X-ray structure at 293 K) is very similar (see Figure 5a and 5b). The higher stability of **2**-LT-0 compared to **2**-HT-0 (the computed cohesive energies per TDPDTA radical for **2**-LT-0 and **2**-HT-0 are 29.4 and 28.7 kcal mol^{-1}, respectively) is consistent with the fact that the former is the observed polymorph at low temperatures.

In summary, the results of the variable cell optimizations demonstrate that the regular π-stacking motif of TDPDTA corresponds to a minimum energy structure in the potential energy surface (PES) of the system, whereas the regular π-stacking motif of PDTA does not.

After having revealed the surprising differences between the structural properties of the π-stacks of **1**-HT and **2**-HT, we will now investigate whether these differences arise from intermolecular interactions within the π-stacks or from

intermolecular interactions between different π-stacks (*i.e.*, those arising from lateral contacts between stacks). To this end, we will analyze the results obtained from optimizations of isolated π-stacks. The optimization of an isolated regular π-stack of PDTA radicals resulted again in a dimerized stack (see Figure 4c and compare to Figure 4b). Conversely, the regular π-stacking pattern observed in the X-ray structure of **2**-HT was preserved upon optimization of an isolated π-stack of TDPDTA radicals (see Figure 5c). It thus follows that the structural properties of the π-stacks of **1**-HT and **2**-HT (specifically, whether or not the uniform stacks are minimum energy configurations at 0 K) are governed by the intra-stack interactions between radicals. That said, the effect of lateral contacts between columns is certainly not negligible because the structure adopted by the π-stacks in the solid state differ significantly from the structure of the isolated π-stacks for both **1** and **2** (see Figures 4 and 5).

3. Dynamics of the HT polymorphs of PDTA and TDPDTA

The role of thermal fluctuations in shaping the structure of the π-stacks of **1**-HT and **2**-HT was explored by means of *ab initio* molecular dynamics (AIMD) simulations conducted at room temperature. The time-resolved evolution of the distance between the nitrogen atoms of the S-N-S moieties of adjacent radicals (N*-N* distance, see Figure 2) in one column of **1**-HT shows that each pair of molecules presents roughly the same kind of large-amplitude intermolecular vibrations around the same mean value (see Figure 6a). In fact, the average structure obtained from the AIMD simulations of **1**-HT contains uniform π-stacks (see Figure 6b), whose structure is very close to the regular structure observed in X-ray crystallography (see Figure 4a). Thermal fluctuations at room temperature thus transform the dimerized columns of the minimum energy configuration of **1**-HT into regular columns. A close inspection into the AIMD trajectories reveal that this transformation is achieved by means of the so-called *pair-exchange dynamics* (PED) mechanism, previously detected in the HT polymorphs of TTTA[65] and 4-NCBDTA[66]. When this mechanism is operative, each radical continually exchanges the adjacent neighbor (upper or lower) with which it forms a dimer. This

mechanism, which takes place in the picosecond timescale, renders all radicals within a stack equivalent, thereby explaining the regular stacking motif detected experimentally.

The AIMD simulations of **2**-HT furnished an average structure presenting also uniform π-stacks, with a structure in very good agreement with the X-ray data (see Figure 6e and 5a). Yet, the amplitude of the intermolecular vibrations in **2**-HT is much smaller than in **1**-HT (compare Figure 6d with Figure 6a). As a result, the computed thermal ellipsoids of **1**-HT are much larger than those of **2**-HT (compare Figures 6c and 6f). Importantly, the experimental thermal ellipsoids show the same trend. In fact, it should be mentioned that the very good agreement between the computed and experimental thermal ellipsoids for both **1**- and **2**-HT (see Figures S7 and S8), together with the very good agreement between the average and X-ray structures, demonstrate that our AIMD simulations properly captured the dynamics of the systems under investigation.

The AIMD simulations of the LT phases of **1** and **2**, in turn, showed that their π-dimers are preserved at finite temperatures (see Figure S9). The resulting average structures and computed thermal ellipsoids for the LT phases are also in very good agreement with the experimental data (see Figures S7 and S8).

The different sizes of the thermal ellipsoids of the atoms of the PDTA and TDPDTA radicals in **1**-HT and **2**-HT stem from the fact that PED is active in the former and not in the latter. As explained in the previous section, the regular π-stacking motif of **2**-HT is already stable at 0 K. Therefore, each of its constituent radicals fluctuates with small-amplitude vibrations around the spatial position dictated by the regular minimum energy configuration without featuring any PED with their nearest neighbors. The comparison between the experimental thermal ellipsoids of **1**-HT and **2**-HT indicates (see Table S1 and Figures S7 and S8) that the size of thermal ellipsoids can be taken as a signature of whether or not a DTA-based crystal exhibits PED. The larger size of the thermal ellipsoids of TTTA compared to those of TDPDTA, which exhibits PED too[65], further corroborates this conclusion (see Table S1).

The different evolution of the dynamics of **1**-HT and **2**-HT as a function of temperature provides additional evidence of the presence/absence of PED. Around room temperature, the probability distribution functions (PDFs) associated with the N*-N* distance for both **1**-HT and **2**-HT are single-peaked (see Figure 7). This means that, at this temperature, the regular π-stacks are the most probable arrangements. Upon cooling, the only change observed in the PDF of **2**-HT is a narrowing of its single peak due to the smaller amplitude of the thermal fluctuations. On the contrary, the single peak of **1**-HT at room temperature splits into two peaks upon cooling (see Figure 7). This behavior, which was previously observed in TTTA[65] and 4-NCBDTA[66], results from the freezing of PED at low temperatures. Once the PED is frozen, the regular π-stacks transform into dimerized stacks, whose alternating long and short intermolecular contacts give rise to the bimodal PDF.

4. Rationalizing the AIMD results

The results of the AIMD simulations can be rationalized on the basis of the potential energy profiles displayed in Figure 8. The energy profile shown for TDPDTA is the computed minimum energy path connecting two different arrangements of an isolated π-stack of TDPDTA radicals: a dimerized configuration and a regular configuration. This profile, whose associated reaction coordinate involves mainly changes in the degree of longitudinal slippage (d_{LG}) and in the values of interplanar distances between adjacent radicals, clearly demonstrates that both arrangements are minimum energy configurations and that the transformation of the regular arrangement into the dimerized arrangement entails an energy barrier. This explains the stability of the regular π-stacks observed in both the AIMD simulations and the geometry optimizations. The energy profile displayed for PDTA, in turn, is the computed minimum energy path connecting two degenerate dimerized configurations: $(\cdots A\text{–}A\cdots A\text{–}A\cdots)_n$ and $(\text{-}A\cdots A\text{–}A\cdots A\text{-})_n$. In this specific case, the associated reaction coordinate involves mainly changes in the degree of latitudinal slippage (d_{SL}) and in the values of interplanar distances between adjacent radicals. In contrast with the scenario found for TDPDTA, the

PDTA profile shows that the regular π-stack $(\cdot\cdot A\cdots A\cdots A\cdots A\cdot\cdot)_n$ is not a minimum energy configuration but a saddle point connecting the two dimerized configurations. This profile also demonstrates that the PED observed in **1**-HT results in fact from a dynamic interconversion between the two degenerate dimerized configurations: $(\cdots A–A\cdots A–A\cdots)_n \leftrightarrow (\text{-}A\cdots A–A\cdots A\text{-})_n$. As already seen in Figure 7, this dynamic interconversion is active only when the system has enough thermal energy to overcome the barrier separating the two dimerized minima.

The results thus far presented reveal two different mechanisms of stabilization of regular π-stacks of DTA radicals. The first mechanism, operative in **1**-HT, furnishes uniform π-stacks by means of a PED process, which is based on a dynamic interconversion between two degenerate dimerized configurations. Hence, the first mechanism relies on dynamical effects to make regular π-stacks stable above a given temperature. Conversely, in the second mechanism, operative in **2**-HT, the stability of regular π-stacks arises exclusively from the potential energy surface of the system at 0 K and does not rely on any dynamical effect.[67]

Having established the existence of these two mechanisms, the key question that needs to be addressed is: which factors determine which is the underlying stabilization mechanism in a given system? So far, the PED-assisted stabilization mechanism has been observed in **1**-HT, TTTA[65] and 4-NCBDTA[66]. In the regular π-stacks of all these systems, the radicals present a significant latitudinal slippage (d_{SL}) with respect to their nearest neighbors (see Figure 2), while the corresponding longitudinal slippage (d_{LG}) is virtually zero. The mechanism based on a locally stable minimum energy configuration, in turn, has only been observed in **2**-HT, for which both latitudinal and longitudinal slippages are important (see Figure 3). It may then be concluded that the type of slippage featured by the radicals in regular π-stacks defines the underlying mechanism of stabilization: the exclusive presence of a latitudinal slippage gives rise to the PED-assisted stabilization mechanism, while the combined presence of latitudinal and longitudinal slippages gives rise to the stabilization mechanism based on a minimum energy configuration at 0 K. The detailed inspection of the

intermolecular interaction in π-dimers of DTA radicals presented in the next subsection supports this conclusion.

5. Intermolecular interactions in π-dimers of DTA radicals

In this subsection, it will be shown that the differences in the structural and dynamical properties of **1**-HT and **2**-HT can be traced back to the properties of the PES of an isolated pair of radicals forming a π-dimer. Figure 9 shows the PES of an isolated π-dimer of TDPDTA radicals as a function of the d_{SL} and d_{LG} variables, while keeping the rest of the structural variables fixed. The exploration of the PES was initially carried out at a fixed interplanar distance of d_{IP} = 3.3 Å, which is the value that results from the variable cell optimization of **2**-HT-0. As might have been anticipated, the 2D-PES exhibits a minimum in the region associated with the π-dimers observed in the LT polymorph of **2**. This minimum on the 2D-PES is located at d_{SL}≈0.6 Å and d_{LG}≈0.0 Å (point A on the map of Figure 9). An increase of d_{SL} while keeping d_{LG} at 0.0 Å results in a monotonic increase of the energy of the 2D-PES (see Figure 9), which means that there is not any other alternative minimum for larger degrees of latitudinal slippage and zero longitudinal slippage. In contrast, a new minimum emerges on the 2D-PES upon increasing simultaneously d_{SL} and d_{LG}. Remarkably, this minimum, located at d_{SL}≈1.8 Å and d_{LG}≈2.1 Å (point C on the map of Figure 9), clearly corresponds to the arrangement of the slipped pairs of radicals present in the regular π-stacks of **2**-HT. It can thus be concluded that the stability of these stacks at 0 K originates in the stability of the latitudinally and longitudinally-slipped arrangement of their constituting pairs. It is worth mentioning that 2D-PESs computed at other values of d_{IP} confirm the existence of these two different minima (A and C in Figure 9) in the subspace spanned by d_{SL} and d_{LG} (see Figure S10).

The larger attractive interaction energy between radicals in configuration A compared with configuration C (see Figure 9) is consistent with the higher stability of **2**-LT-0 compared with **2**-HT-0. The interaction energy decomposition analysis performed for these two configurations (see Table S2) reveals two important aspects. First, the dominant attractive components of the interaction energy in

configuration A are dispersion and polarization (which is associated with the SOMO-SOMO bonding interaction), in agreement with the reported properties of pancake bonding between π-radicals.[39,42,43, 68] Second, all the attractive components of the interaction energy become substantially smaller in going from A to C. This is, however, accompanied with a very large reduction of the repulsive component of the interaction energy, and this explains why configuration C is just slightly less stable than A.

Although the results obtained from the exploration of the 2D-PES of a π-dimer of PDTA radicals are similar to those obtained for TDPDTA radicals (see Figure S11 and Table S3), there are two important differences between the two systems that should be underscored. First, the minimum associated with configuration A in the case of PDTA does not feature any type of slippage, which is consistent with the presence of nearly eclipsed π-dimers in **1**-LT. Like in the case of TDPDTA, an increase of d_{SL} while keeping d_{LG} fixed at 0.0 Å does not lead to any new minimum. This explains why the regular stacks of **1**-HT are unstable against a dimerization process at 0 K. Additionally, the energy difference between configurations A and C in PDTA is higher than in TDPDTA (in fact, it is more than doubled, see Figure S12). This might well explain - at least, partially- why no polymorph comprising latitudinally- and longitudinally slipped pairs of PDTA radicals has been observed yet.

Overall, the results presented in this subsection demonstrate that the structural properties of π-stacks of DTA radicals can be rationalized on the basis of the intermolecular interactions of their constituting π-dimers. Therefore, a detailed knowledge of the energetically favorable π-stacking geometries of DTA dimers can be very useful when it comes to predicting crystal structures of DTA-based compounds and to designing new architectures based on π-stacks of radicals with the desired properties.

Conclusions

The computational study herein presented has demonstrated that regular π-stacks of planar DTA radicals can be rendered stable in some range of temperatures through two different mechanisms. One of the stabilization mechanisms is operative when the configuration exhibiting regular π-stacks is associated with a locally stable minimum in the PES of the system (*i.e.*, a minimum energy configuration at 0 K). Alternatively to this *static* mechanism, another stabilization mechanism occurs based on a dynamic interconversion between two degenerate dimerized configurations. This *dynamic* mechanism is operative when the configuration exhibiting regular π-stacks is not a minimum on the PES, but a minimum on the free energy surface of the system. The data gathered so far indicate that the type of mechanism operative in a given uniform π-stack depends on the type of slippage exhibited by its adjacent DTAs: when each radical in a stack exhibits solely a latitudinal slippage with respect to its neighbors, the underlying stabilization mechanism is the *dynamic* mechanism; conversely, when each radical exhibits both latitudinal and longitudinal slippages with respect to its neighbors, the underlying stabilization mechanism is the *static* mechanism.

The discovery of two distinct stabilization mechanisms in the family of DTAs is relevant for several reasons. First, a detailed knowledge of which stabilization mechanism is active in a given DTA-based material is essential for the proper interpretation of its physical properties because the impact of thermal fluctuations on these properties can be larger in the regular π-stacks stabilized by means of the *dynamic* mechanism. Indeed, it has already been demonstrated that the large-amplitude thermal fluctuations associated with the *dynamic* mechanism have a notable impact on the magnetic properties of TTTA.[69]

Second, this discovery is also relevant in the context of DTA-based molecular crystals with switchable magnetic properties. Indeed, the existence of two different stabilization mechanisms results, in turn, in two distinct mechanisms of exploiting phase transitions between dimerized and regular π-stacks of DTAs to endow this type of materials with spin-switching properties. When the stability of

regular stacks arises from the *dynamic* mechanism, the spin transition originates in the thermal promotion of a dynamic interconversion between two degenerate dimerized configurations. Thus, the key parameter that controls the phase transition temperature is the energy barrier separating the two degenerate configurations. 4-NCBDTA is the prototypical example of this switching mechanism. Note that the underlying mechanism of the hysteretic phase transition of PDTA and TTTA is more complex because the promotion of the dynamic interconversion is accompanied by a rearrangement of the intermolecular bonds between the π-stacks. In contrast, in the case of a regular stack stabilized by means of the *static* mechanism, the key parameter controlling the phase transition temperature is the energy difference between the two different minimum energy configurations, namely a LT and HT phase with dimerized and uniform π-stacks, respectively. This does not mean that the energy barrier between these two configurations can be ignored, since this barrier might play a role in shaping the characteristics of the phase transition (e.g. by opening a hysteresis loop). In any case, it is clear that the parameters that need to be considered when designing switchable DTA-based materials are different depending on the stabilization mechanism of regular π-stacks that one wants to exploit. TDPDTA is thus far the only DTA radical whose spin transition is based on the *static* stabilization mechanism. In view of the hysteretic character of this spin transition, it is clear that the search for other DTA radicals undergoing the same type of spin transitions might well result in new switchable materials with very interesting properties. In this respect, the quest for new planar DTA radicals that pack forming latitudinally and longitudinally-slipped π-stacks looks promising. In terms of potential design rules for this type of radicals, the results so far obtained suggest that the fused rings to the dithiazolyl ring should be chosen in such a way that they have a slight preference for a slipped π-π stacking interaction, thereby partially counteracting the driving force of the SOMO-SOMO overlap of the dithiazolyl moiety for an eclipsed configuration. Should the fused rings favor the eclipsed configuration, this configuration would be much more stable than a latitudinally and longitudinally slipped configuration, thus preventing the latter from being observed in the solid state.

On the whole, the results here reported provide valuable information for the interpretation of the structural and physical properties of DTA-based crystals. In addition, the correlation between the type of slippage between adjacent radicals and the type of stabilization mechanism, together with the fact that the preference for one type of slippage or the other can be inferred simply from the PES of π-dimers should facilitate the design of new DTA materials based on π-stack architectures. Future studies will address whether the two different stabilization mechanisms herein disclosed are also operative in other families of planar organic radicals.

Methods

2. Minimum energy configurations of the LT and HT polymorphs of PDTA and TDPDTA

The variable-cell geometry optimizations of the LT and HT polymorphs of **1** and **2** were performed by means of the CP2K[70] code at DFT level, using the PBE[71,72] functional within the spin unrestricted formalism, taking advantage of the Orbital Transformation[73] algorithm as implemented in the Quickstep[74,75] module. Norm-conserving Goedecker-Teter-Hutter[76,77,78] pseudopotentials were employed for all the atomic species, in combination with a TZV2P basis set[79] (specifically optimized for accurate molecular calculations) and a Γ-point sampling of the Brillouin zone. A 600 Ry cutoff was used for truncating the plane waves expansion. Grimme's D3[80] dispersion potential was added to the Kohn-Sham (KS) DFT energy in order to account for the van der Waals intermolecular interactions. It is noted that previous works have demonstrated that the use of PBE and Grimme's schemes for dispersion corrections perform very well when it comes to simulating π-stacked architectures of DTA radicals[65,66] and π-dimers of other radicals[81]. The optimizations of isolated π-stacks (in which periodic boundary conditions along the stacking direction were considered) were done using the same electronic structure setup as the one employed for the variable-cell geometry optimizations.

3. Dynamics of the HT polymorphs of PDTA and TDPDTA

Ab Initio Molecular Dynamics (AIMD) simulations were performed making use of the CP2K code[70], with the same electronic structure settings used for the variable-cell geometry optimizations (see the previous subsection), within the Born-Oppenheimer approach. The AIMD simulations were performed using the *NVT* canonical ensemble, by employing a velocity rescaling stochastic algorithm (CSVR) thermostat[82] and a time-step of 1 femtosecond. The thermal equilibrations of the structures of **1** and **2** were performed for 3 picoseconds each, with a subsequent production run of *circa* 10 ps.

The AIMD simulations of **1**-HT and **2**-HT leading to the results displayed in Figure 6 were run at 300 and 293 K, respectively. The dynamics of **1**-HT and **2**-HT at lower temperatures were investigated by means of AIMD simulations run at 150 and 120 K, respectively. The supercell used in the AIMD simulation of **2**-HT-293 was built directly from the X-ray measured unit cell parameters at 293 K. The supercells used in the AIMD simulations of **1**-HT-300, **1**-HT-150 and **2**-HT-120 were not built directly from experimental unit cells because there is no X-ray data at these temperatures. The supercell parameters of **1**-HT-300 and **1**-HT-150 were obtained by means of a linear interpolation between the experimental cell parameters of the **1**-HT-323 X-ray-recorded structure and the cell parameters resulting from the variable-cell geometry optimization of **1**-HT. The supercell parameters of **2**-HT-120 were in turn obtained by means of a linear interpolation between the experimental cell parameters of the **2**-HT-293 X-ray-recorded structure and the cell parameters resulting from the variable-cell geometry optimization of **2**-HT.

4. Rationalizing the AIMD results

The two minimum energy paths displayed in Figure 8 were computed by means of the *Nudged Elastic Band* (NEB) algorithm[83,84] using the NEB module implemented in the Quantum Espresso suite of programs[,85]. These calculations were done using the PBE[71,72] exchange correlation functional within the spin unrestricted formalism, supplemented by Grimme's D2 semiempirical dispersion potential[86]. Ultrasoft Vanderbilt pseudopotentials[87] were employed to describe the atomic species, with a kinetic energy cutoff of 35 Ry for the plane wave expansion and the Γ-point sampling of the Brillouin zone. The NEB profiles in Figure 8 were computed for isolated π-stacks of radicals (each π-stack was composed of four radicals) considering periodic boundary conditions along the stacking direction. The NEB profiles of isolated π-stacks of **1** and **2** were obtained using 12 and 14 intermediate images, respectively.

5. Intermolecular interactions in π-dimers of DTA radicals

The PESs shown in Figures 9, S10 and S11 were computed for isolated π-dimers using the same electronic structure setup as the one employed to calculate the NEB profiles (see previous subsection). The results obtained at the PBE-D2 level were validated using a correlated wavefunction method. Specifically, the minimum energy paths connecting points A, B and C in the 2D-PESs of Figures 9 and S11 were also computed using the NEVPT2 method[88,89], as implemented in the Orca code[90]. The NEVPT2 calculations were carried out using an active space of 10 π-electrons and 10 π-orbitals for the π-dimers of **1**, and an active space of 14 π-electrons and 14 π-orbitals for the π-dimers of **2**, with the def2-TZVP basis set[91]. As can be seen in Figure S12, the NEVPT2 profiles agree quite well with the PBE-D2 profiles and confirm the existence of two different minimum energy configurations of the π-dimers in the subspace spanned by d_{SL} and d_{LG}. It thus follows that the combined use of PBE and Grimme's semiempirical dispersion correction allow for a proper description of the π-interactions between the DTA radicals herein studied.

The interaction energy decomposition analysis performed for points A, B and C of the 2D-PESs of Figures 9 and S11 were carried out using an Energy Decomposition Analysis [92] method that can be applied within the DFT framework [93], as implemented in the GAMESS suite of programs[94]. This analysis was performed at the PBE-D3/cc-PVTZ[95] level using the spin-unrestricted formalism.

Acknowledgements

FM, MD, JJN and JRA acknowledge financial support from MINECO through Grant CTQ2017-87773-P/AEI/FEDER, UE and Spanish Structures Excellence María de Maeztu program through grant MDM-2017–0767. FM, MD, JJN and JRA are also thankful to the Catalan DURSI (2017SGR348 grant) and to BSC and CSUC for the allocation of computer time. TF acknowledges funding from the European Union's Horizon 2020 research and innovation programme under the Marie Curie Skłodowska-Curie grant agreement no. 642294.

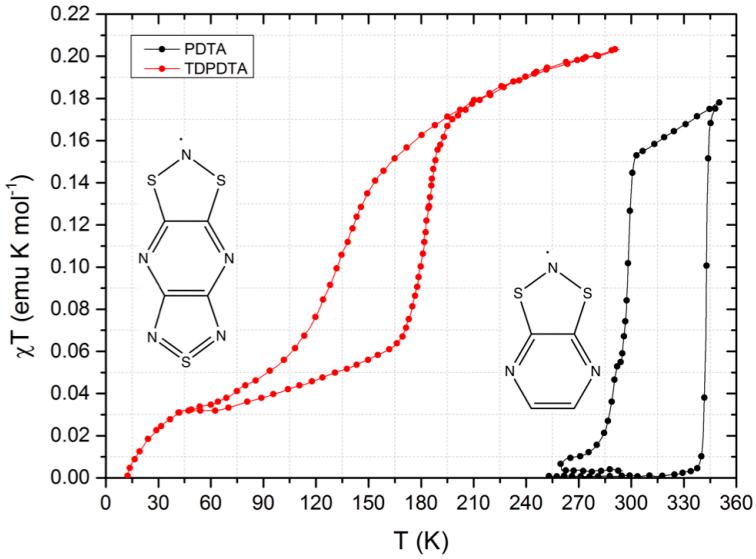

Figure 1. Temperature dependence of χT (χ is the magnetic susceptibility) for PDTA (black) and TDPDTA (red). The insets show the molecular structures of the PDTA (right) and TDPDTA (left) neutral radicals. The χT values of PDTA and TDPDTA were taken from Refs. 45 and 44, respectively.

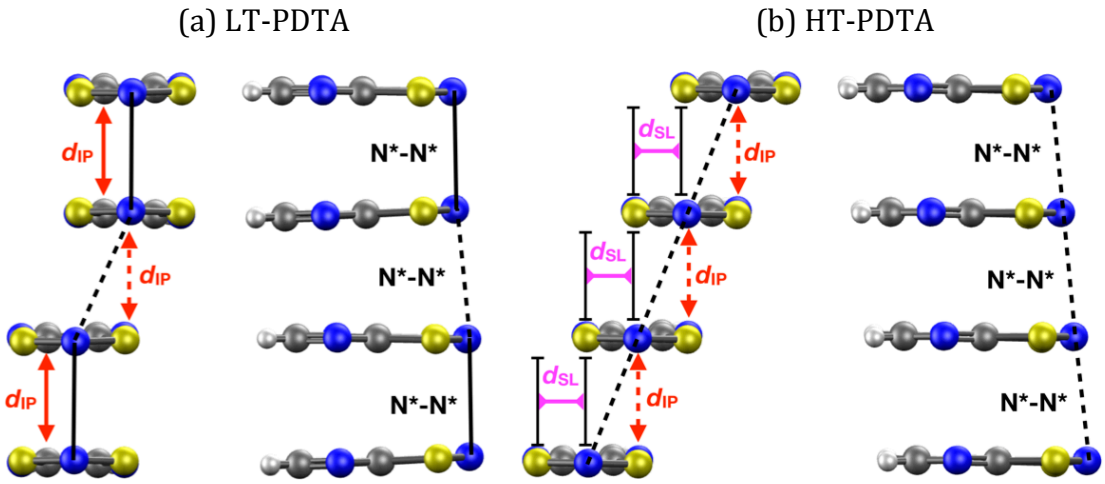

Figure 2. Two side views of one π-stack of the experimental structure of the LT (a) and (b) HT polymorphs of PDTA. The X-ray structures of both polymorphs were obtained at 323 K.[45] The d_{IP} and d_{SL} variables measure the interplanar distance between adjacent radicals and the degree of latitudinal slippage between adjacent radicals, respectively.

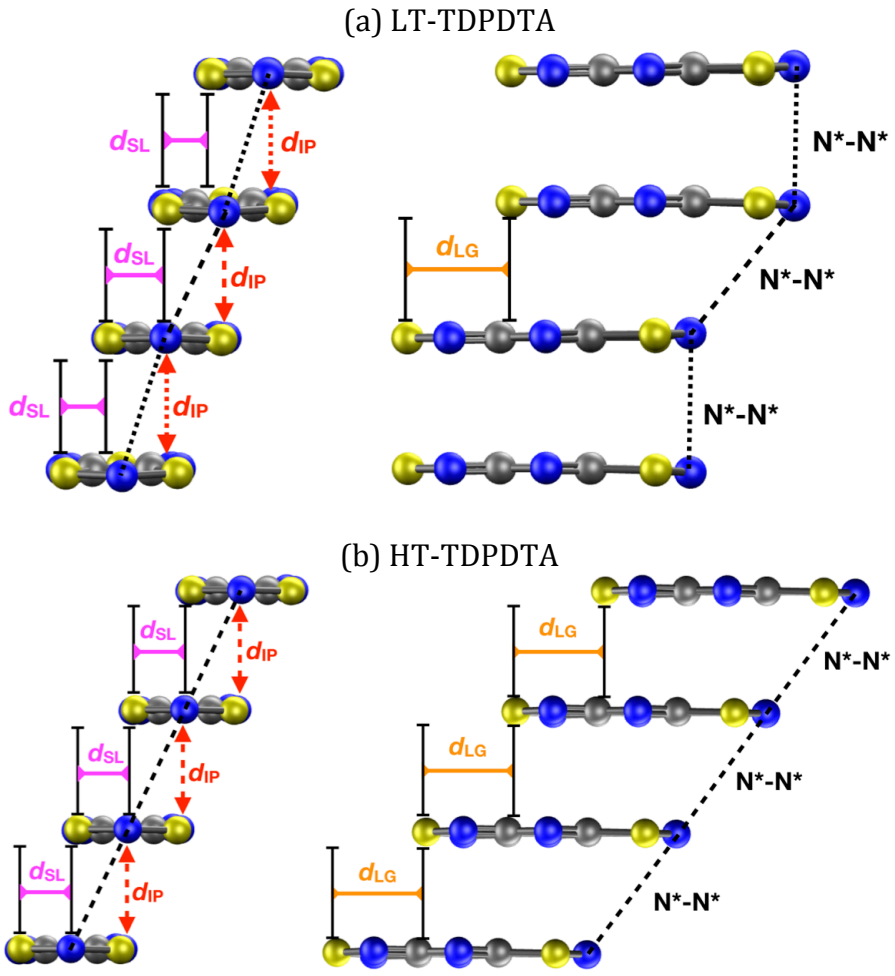

Figure 3. Two side views of one π-stack of the experimental structure of the LT (a) and (b) HT polymorphs of TDPDTA. The X-ray structures of both polymorphs were obtained at 150 and 293 K, respectively. The d_{IP}, d_{SL} and d_{LG} variables measure the interplanar distance between adjacent radicals, the degree of latitudinal slippage between adjacent radicals, and the degree of longitudinal slippage, respectively.

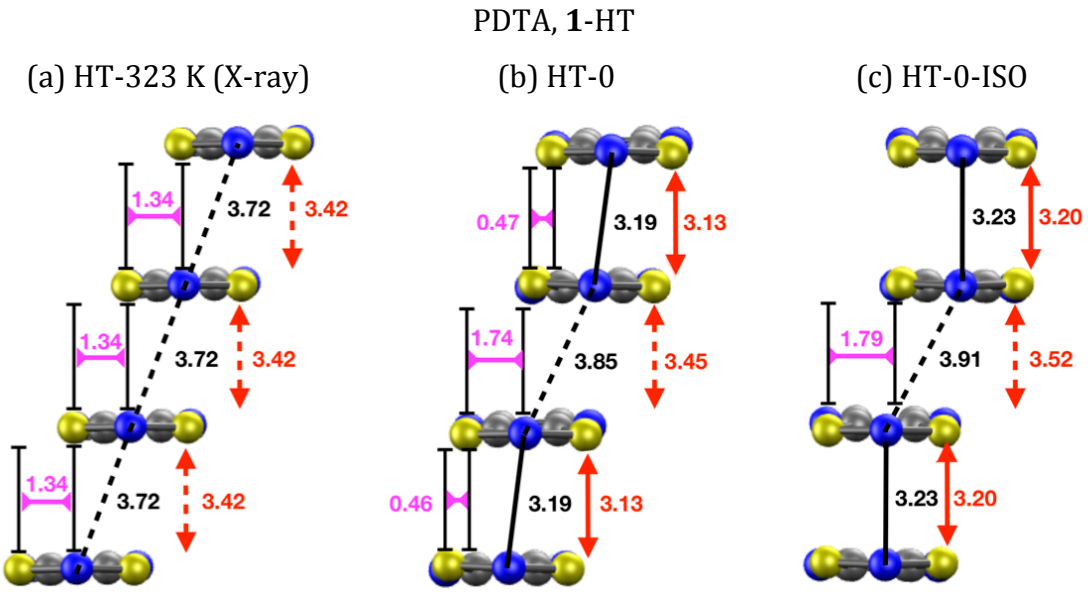

Figure 4. Side view of one π-stack of the HT polymorph of **1**. The figure displays (*a*) the X-ray structure at 323 K, (*b*) the optimized structure at 0 K and (*c*) the optimized structure at 0 K of one isolated stack. The black, red and purple values shown in the image mark the distances between the nitrogen atoms of the S-N-S moieties of adjacent radicals, the interplanar distance (d_{IP}) between adjacent radicals and the degree of latitudinal slippage between adjacent radicals (d_{SL}), respectively.

TDPDTA, **2**-HT

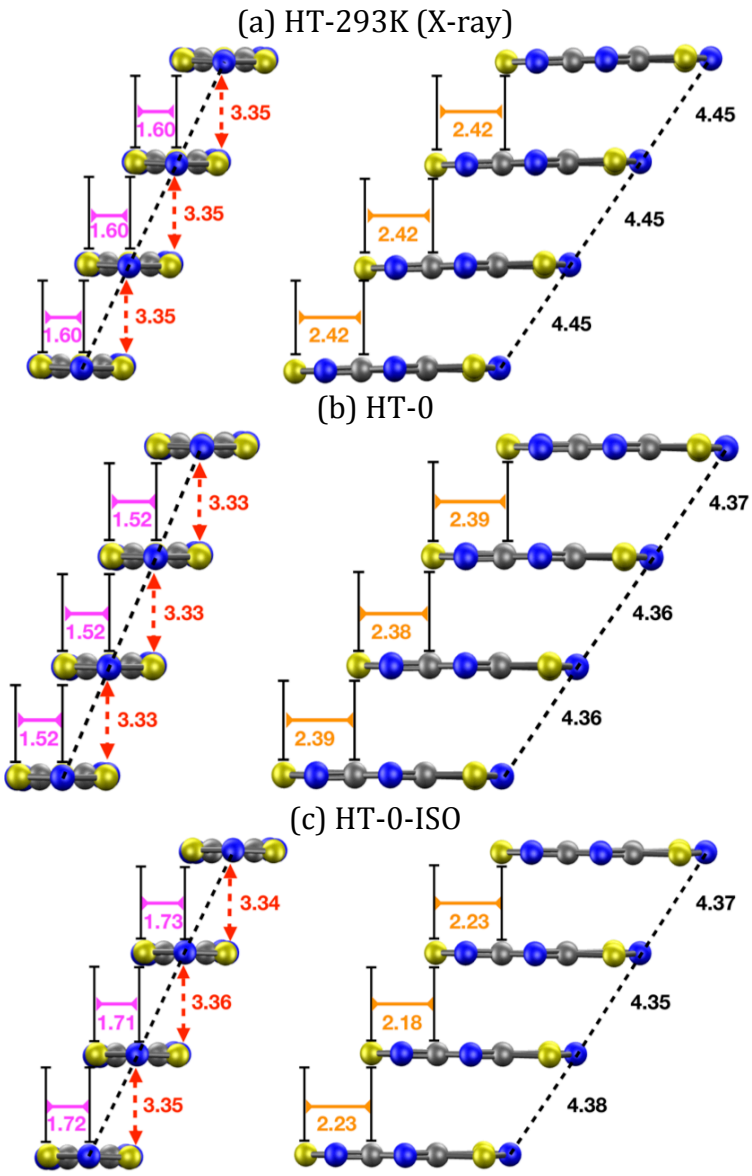

Figure 5. Two side views of one π-stack of the HT polymorph of **2**. The figure displays (*a*) the X-ray structure at 293 K, (*b*) the optimized structure at 0 K and (*c*) the optimized structure at 0 K of one isolated stack. The black, red, purple and orange values shown in the image mark the distances between the nitrogen atoms of the S-N-S moieties of adjacent radicals, the interplanar distance between adjacent radicals (d_{IP}), the degree of latitudinal slippage between adjacent radicals (d_{SL}), and the degree of longitudinal slippage (d_{LG}), respectively.

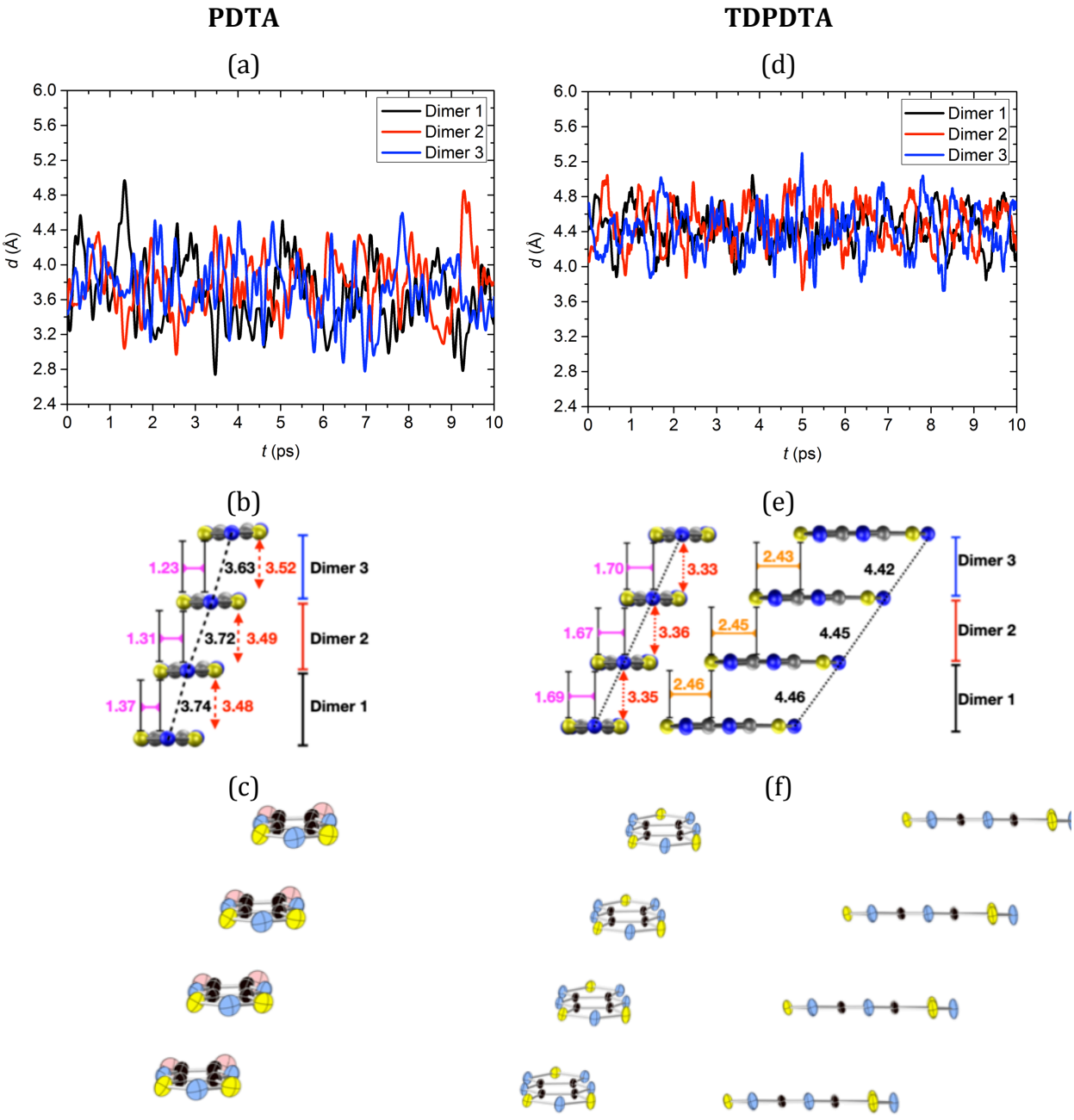

Figure 6: Results of the AIMD simulations of **1**-HT-300 (the HT polymorph of PDTA simulated at 300 K, *a*-*c*) and **2**-HT-293 (the HT polymorph of TDPDTA simulated at 293 K, *d*-*f*). The panel shows: the time-resolved evolution of the distance between the nitrogen atoms of the S-N-S moieties of adjacent radicals in one column of (*a*) **1**-HT-300 and one column of (*d*) **2**-HT-293; the average structure of one stack for both (*b*) **1**-HT-300 and (*e*) **2**-HT-293 as obtained from the AIMD simulations; and the computed thermal ellipsoids for both (*c*) **1**-HT-300 and (*f*) **2**-HT-293. Note that two different side views of one stack are displayed in the (*e*) and (*f*) panels.

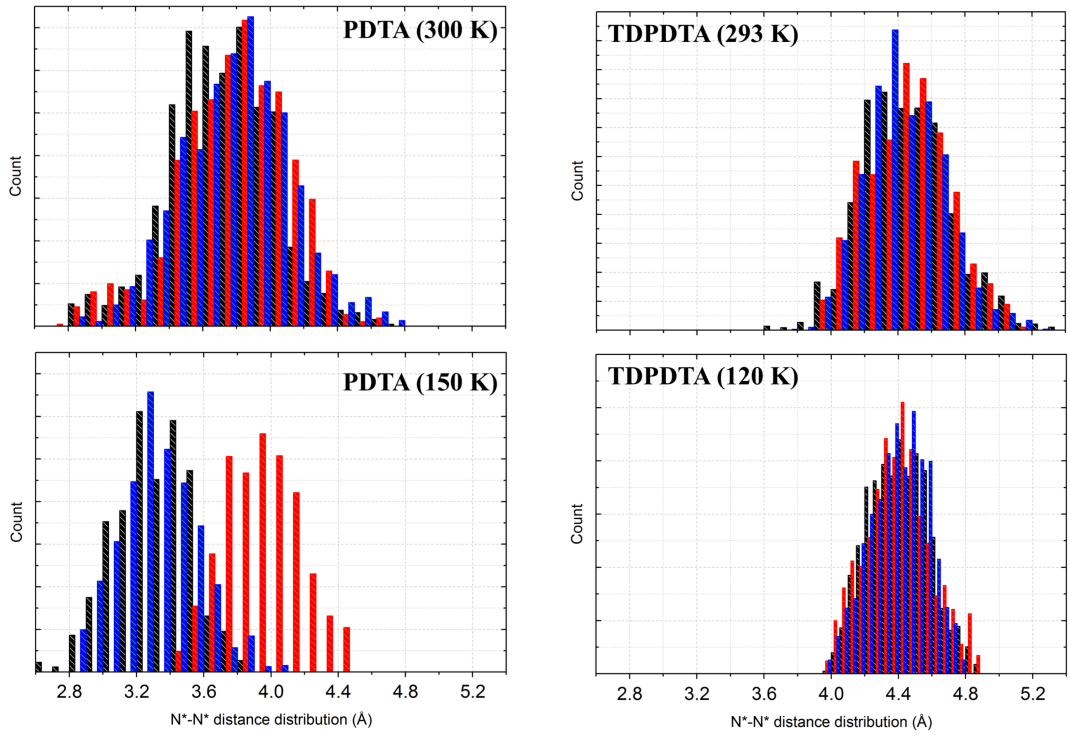

Figure 7: Temperature-dependence of the dynamics in **1**-HT and **2**-HT. The figure displays the probability distribution functions (PDFs) associated with the N*-N* distance at two different temperatures for each material. The PDFs were obtained from the configurations sampled along the AIMD simulations. Color code: dimers 1, 2 and 3 in black, red and blue, respectively (see Figure 6 for labelling of dimers).

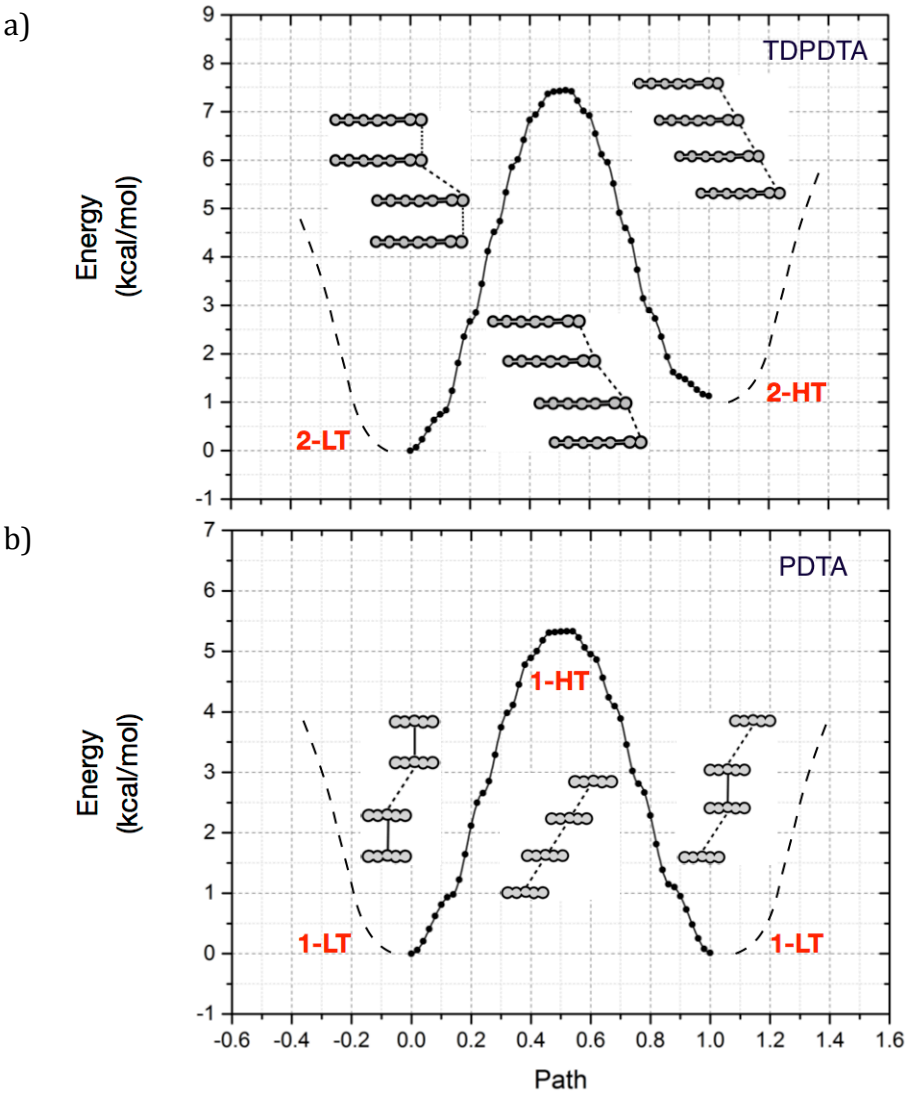

Figure 8: (*a*) Minimum energy path connecting a dimerized π-stack (minimum on the left) with a regular π-stack (minimum on the right) of TDPDTA. (*b*) Minimum energy path connecting two degenerate dimerized π-stacks of PDTA. The maximum of the path in (*b*) is associated with the regular arrangement of radicals. The solid lines connecting the black dots are meant to guide the eye. The dashed lines of the profiles do not correspond to any calculation, but they are meant to emphasize the existence of minimum energy configurations.

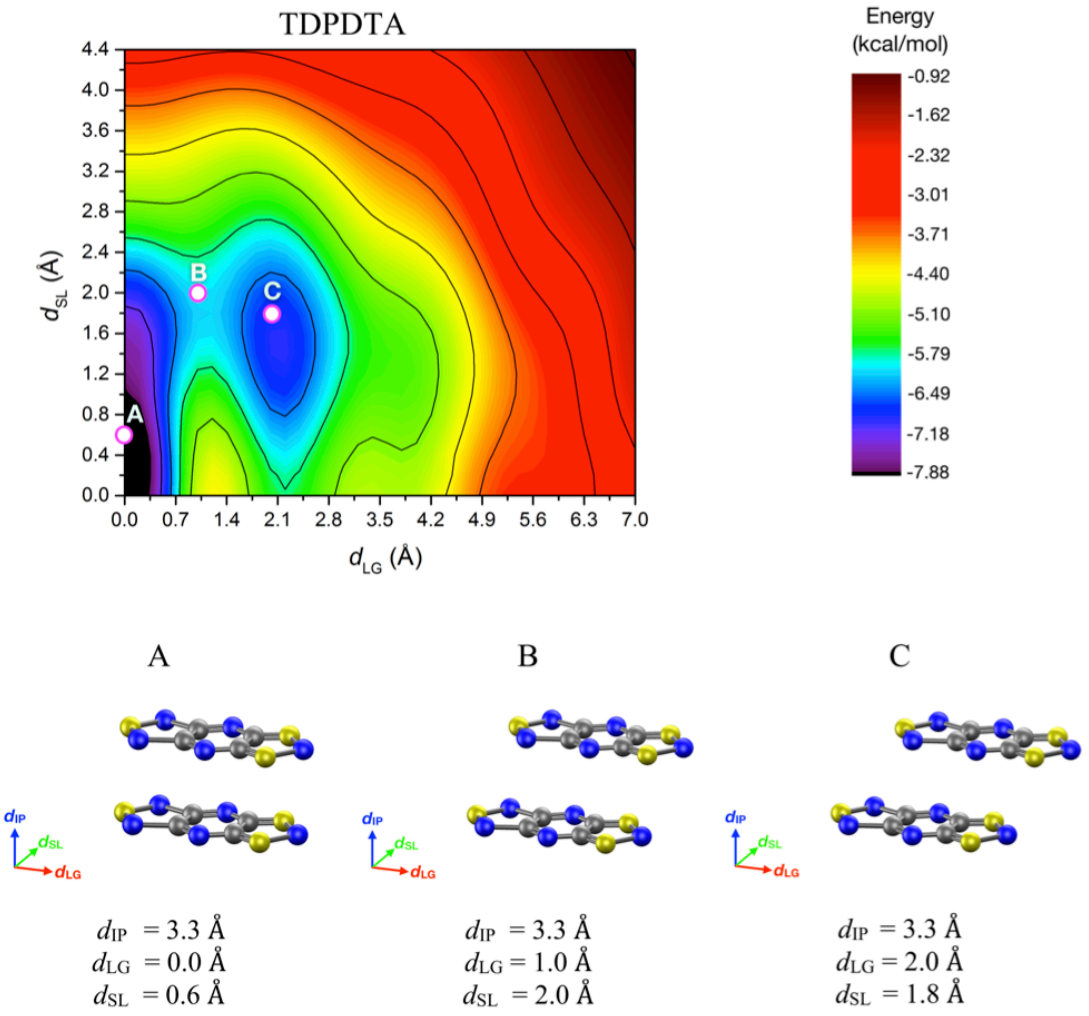

Figure 9: Potential energy surface of an isolated π-dimer of TDPDTA radicals as a function of the degree of latitudinal slippage (d_{SL}) and the degree of longitudinal slippage (d_{LG}), while keeping fixed the interplanar distance (d_{IP}) at a value of 3.3 Å. The values of the energies refer to interaction energies between the two radicals. The configurations associated with the A, B and C points marked on the color map are displayed at the bottom of the figure. The values of the d_{SL} and d_{LG} variables for each of these configurations are also shown.

References

[1] K. Molčanov, B. Kojić-Prodić, *IUCrJ*, 2019, **6**, 156-166.

[2] J. S. Miller, *Adv. Mater*., 2002, **14**, 1105–1110.

[3] R. G. Hicks, *Org. Biomol. Chem*., 2007, **5**, 1321–1338.

[4] Stable radicals: fundamentals and applied aspects of odd-electron compounds, (Ed. R. G. Hicks), John Wiley & Sons, **2011**.

[5] P. M. Lahti, *Adv. Phys. Org. Chem*., 2011, **45**, 93–169.

[6] I. Ratera and J. Veciana, *Chem. Soc. Rev.*, 2012, **41**, 303–349.

[7] S. M. Winter, S. Hill, and R. T. Oakley, *J. Am. Chem. Soc*. 2015, **137**, 3720−3730.

[8] J. Zapata-Rivera, D. Maynau, and C. J. Calzado, *Chem. Mater*., 2017, **29**, 4317−4329

[9] R.C. Haddon, *Nature*, 1975, **256**, 394–396.

[10] E. Coronado, P. Day, *Chem. Rev*. 2004, **104**, 5419 – 5448.

[11] J. M. Rawson, A. Alberola, and A. Whalley, *J. Mater. Chem*., 2006, **16**, 2560–2575.

[12] M. Vérot, J-B. Rota, M. Kepenekian, B. Le Guennic, and V. Robert, *Phys. Chem. Chem. Phys*., 2011, **13**, 6657–6661.

[13] K. Yoneda, M. Nakano, K. Fukuda, H. Matsui, S. Takamuku, Y. Hirosaki, T. Kubo, K. Kamada, and B. Champagne, *Chem. Eur. J.*, 2014, **20**, 11129 – 11136.

[14] H. Matsui, M. Yamane, T. Tonami, M. Nakano, M. de Wergifosse, T. Seidler, and B. Champagne, *J. Phys. Chem. C.*, 2018, **122**, 6779−6785.

[15] Y. Morita, T. Murata, K. Nakasuji, *Bull. Chem. Soc. Jpn*., 2013, **86**, 183-197.

[16] H. Endres in *Extended Linear Chain Compounds Vol. 3*, , Ed. J.S. Miller, Springer, Plenum Press, New York, 1983, 263 – 312.

[17] X. Chen, F. Gao and W. Yang, *Sci. Rep*., 2016, **6**, 29314.

[18] K. Molčanov, V. Stilinović, A. Šantić, N. Maltar-Strmečki, D. Pajić, and B. Kojić-Prodić, *Cryst. Growth Des*., 2016, **16**, 4777−4782.

[19] K. Molčanov, Z. Mou, M. Kertesz, B. Kojić-Prodić, D. Stalke, S. Demeshko, A. Šantić, V. Stilinović, *Chem. Eur. J*., 2018, **24**, 8292-8297.

[20] R. G. Hicks, M.T. Lemaire, L. Öhrström, J.F. Richardson, L.K. Thompson, and Zhiqiang Xu, *J. Am. Chem. Soc*., 2001, **123***,* 7154-7159.

[21] L. Norel, J-B. Rota, L-M. Chamoreau, G. Pilet, V. Robert, and C. Train, *Angew. Chem. Int. Ed*., 2011, **50**, 7128 –7131.

[22] S. K. Pal, M. E. Itkis, R. W. Reed, R. T. Oakley, A. W. Cordes, F. S. Tham, T. Siegrist, and R. C. Haddon, *J. Am. Chem. Soc*., 2004**, 126**, 1478-1484.

[23] P. A. Koutentis, Y. Chen, Y. Cao, T. P. Best, M. E. Itkis, L. Beer, R. T. Oakley, A. W. Cordes, C. P. Brock, and R. C. Haddon, *J. Am. Chem. Soc*., 2001, **123**, 3864-3871.

[24] B. Yan, J. Cramen, R. McDonald and N. L. Frank, *Chem. Commun*., 2011, **47**, 3201–3203.

[25] C. P. Constantinides, P. A. Koutentis, and J. M. Rawson, *Chem. Eur. J*., 2012, **18**, 7109 – 7116.

[26] Y. Le Gal, T. Roisnel, P. Auban-Senzier, N. Bellec, J. Íñiguez, E. Canadell, and Dominique Lorcy, *J. Am. Chem. Soc*., 2018, **140**, 6998−7004.

[27] A. Mizuno, H. Benjamin, Y. Shimizu, Y. Shuku, M. M. Matsushita, N. Robertson, and K. Awaga, *Adv. Funct. Mater.* 2019, 1904181.

[28] A. W. Cordes, R. C. Haddon, R. G. Hicks, R. T. Oakley, T. T. M. Palstra, L. F. Schneemeyer, and J. V. Waszczak, *J. Am. Chem. Soc*., 1992, **114**, 5000 – 5004.

[29] D.A. Haynes, *CrystEngComm*, 2011, **13**, 4793 – 4805.

[30] Y. Beldjoudi, R. Sun, A. Arauzo, J. Campo, R. J. Less, and J.M. Rawson, *Cryst. Growth Des.*, 2018, **18**, 179−188.

[31] Y. Beldjoudi, M. A. Nascimento, Y. J. Cho, H. Yu, H. Aziz, D. Tonouchi, K. Eguchi, M. M. Matsushita, K. Awaga, I. Osorio-Roman, C. P. Constantinides, and J. M. Rawson, *J. Am. Chem. Soc*., 2018, **140**, 6260−6270.

[32] T.M. Barclay, A.W. Cordes, N.A. George, R.C. Haddon, R.T. Oakley, T. T. M. Palstra, G. W. Patenaude, R.W. Reed, J.F. Richardson and H. Zhang, *Chem. Commun*., 1997, 873 – 874.

[33] W. Fujita and K. Awaga, *Science*, 1999, **286**, 261 – 262.

[34] J. L. Brusso, O. P. Clements, R. C. Haddon, M. E. Itkis, A. A. Leitch, R. T. Oakley, R. W. Reed and J. F. Richardson, *J. Am. Chem. Soc*., 2004, **126**, 8256–8265.

[35] L. Beer, J.L. Brusso, A.W. Cordes, R.C. Haddon, M.E. Itkis, K. Kirschbaum, D.S. MacGregor, R.T. Oakley, A. Pinkerton, and R. W. Reed, *J. Am. Chem. Soc*., 2002, **124**, 9498-9509.

[36] X. Yu, A. Mailman, K. Lekin, A. Assoud, C. M. Robertson, B. C. Noll, C.F. Campana, J.A. K. Howard, P.A. Dube, R.T. Oakley, *J. Am. Chem. Soc*., 2012, **134**, 2264–2275.

[37] A. Mailman, J.W.L. Wong, S.M. Winter, R.C.M. Claridge, C.M. Robertson, A. Assoud, W. Yong, E. Steven, P.A. Dube, J.S. Tse, S. Desgreniers, R. A. Secco, and R. T. Oakley, *J. Am. Chem. Soc*., 2017, **139**, 1625–1635.

[38] A. Mailman, C.M. Robertson, S.M. Winter, P.A. Dube, and R. T. Oakley, *Inorg. Chem*., 2019, **58**, 6495-6506.

[39] J.S. Miller, J.J. Novoa, *Acc. Chem. Res*. 2007, **40**, 189–196.

[40] D. Jose, A. Datta, *Cryst. Growth Des*. 2011, **11**, 3137–3140.

[41] K.E. Preuss, *Polyhedron*, 2014, **79**, 1–15.

[42] Z. Cui, H. Lischka, H.Z. Beneberu, M. Kertesz, *J. Am. Chem. Soc*. 2014, **136**, 12958–12965.

[43] M. Kertesz, *Chem. Eur. J*., 2019, **25**, 400 – 416.

[44] T. M. Barclay, A. W. Cordes, N. A. George, R. C. Haddon, M. E. Itkis, M. S. Mashuta, R. T. Oakley, G. W. Patenaude, R. W. Reed, J. F. Richardson, H. Zhang, *J. Am. Chem. Soc*. 1998, **120**, 352 – 360.

[45] J. L. Brusso, O. P. Clements, R. C. Haddon, M. E. Itkis, A. A. Leitch, R. T. Oakley, R. W. Reed, J. F. Richardson, *J. Am. Chem. Soc*. 2004, **126**, 14692-14693.

[46] A. Alberola, R. J. Collis, S. M. Humphrey, R. J. Less, J. M. Rawson, "Spin Transitions in a Dithiazolyl Radical: Preparation, Crystal Structures, and Magnetic Properties of 3-Cyanobenzo-1,3,2-dithiazolyl,$C_7H_3S_2N_2$•". *Inorg. Chem*., 2006, **45**, 1903–1905.

[47] Y. Lepine, A. Caille, and V. Larochelle, *Phys. Rev. B: Condens. Matter Mater. Phys.,* 1978, **18**, 3585 – 3592.

[48] K. Molčanov, B. Kojić-Prodić, D. Babić, D. Pajić, N. Novosel and K. Zadro, *CrystEngComm*, 2012, **14**, 7958–7964.

[49] R. Suizu, A. Iwasaki, Y. Shuku, K. Awaga, *J. Mater. Chem. C*, 2015, **3**, 7968 – 7977.

[50] H. Matsuzaki, W. Fujita, K. Awaga, H. Okamoto, *Phys. Rev. Lett*. 2003, **91**, 017403.

[51] O. Sato, *Nat. Chem*. 2016, **8**, 644 – 656.

[52] J. M. Rawson, J. J. Hayward in *Spin-Crossover Materials: Properties and Applications*, (Ed. M. A. Halcrow), Wiley, Hoboken, **2013**, pp. 225 – 237.

[53] *Spin-Crossover Materials-Properties and Applications*, (Ed. M. A. Halcrow), Wiley, Hoboken, **2013**.

[54] S. Brooker, *Chem. Soc. Rev*. 2015, **44**, 2880 – 2892.

[55] O. Kahn, C. J. Martinez, *Science* 1998, **279**, 44 – 48.

[56] D. Bates, C.M. Robertson, A.A. Leitch, P.A. Dube, and R.T. Oakley, *J. Am. Chem. Soc*. 2018, **140**, 3846–3849.

[57] K. Lekin, S.M. Winter, L.E. Downie, X. Bao, J.S. Tse, S. Desgreniers, R.A. Secco, P.A. Dube, R.T. Oakley, *J. Am. Chem. Soc*., 2010, **132**, 16212–16224.

[58] K. Lekin, H. Phan, S.M. Winter, J.W.L. Wong, A.A. Leitch, D. Laniel, W. Yong, R.A. Secco, J.S. Tse, S. Desgreniers, P.A. Dube, M. Shatruk, and R.T. Oakley, *J. Am. Chem. Soc.*, 2014, **136**, 8050–8062.

[59] D.A. Shultz, R.M. Fico, Jr., P.D. Boyle, and J.W. Kampf, *J. Am. Chem. Soc*., 2001, **123**, 10403-10404.

[60] M. E. Itkis, X. Chi, A. W. Cordes, R. C. Haddon, *Science* 2002, **296**, 1443 –1445.

[61] M. Fumanal, J.J. Novoa, and J. Ribas-Arino, *Chem. Eur. J*., 2017, **23**, 7772–7784.

[62] M.B. Mills, T. Wohlhauser, B. Stein, W.R. Verduyn, E. Song, P. Dechambenoit, M. Rouzierès, R. Clérac, and K.E. Preuss, *J. Am. Chem. Soc.*, 2018, **140**, 16904–16908.

[63] Y. Beldjoudi, A. Arauzo, J. Campo, E.L. Gavey, M. Pilkington, M.A. Nascimento, and J. M. Rawson, *J. Am. Chem. Soc*., 2019, **141**, 6875–6889.

[64] T. Francese, J. Ribas-Arino, J.J. Novoa, R.W.A. Havenith, R. Broer, C. de Graaf and M. Deumal, *Phys. Chem. Chem. Phys.,* 2018, **20**, 20406 – 20416.

[65] S. Vela, F. Mota, M. Deumal, R. Suizu, Y. Shuku, A. Mizuno, K. Awaga, M. Shiga, J. J. Novoa, J. Ribas-Arino, *Nat. Commun*. 2014, **5**, 4411.

[66] S. Vela, M.B. Reardon, C.E. Jakobsche, M. M. Turnbull, J. Ribas- Arino, and J.J. Novoa, *Chem. Eur. J.,* 2017, **23**, 3479 – 3489.

[67] Note that in the case of TDPDTA, the stability of the regular π-stacks is associated with a local minimum energy configuration in the PES of the system. The dimerized π-stacks are in fact more stable than the regular ones.

[68] Y. Jung, M. Head-Gordon, *Phys. Chem. Chem. Phys*. 2004, **6**, 2008 – 2011.

[69] S. Vela, M. Deumal, M. Shiga, J. J. Novoa, J. Ribas-Arino, *Chem. Sci*., 2015, **6**, 2371-2381.

[70] CP2K v.4.1, J. Hutter, M. Iannuzzi, F. Schiffmann, J. VandeVondele, *WIREs Comput Mol Sci* 2014, **4**:15–25.

[71] J. P. Perdew, K. Burke, M. Ernzerhof, *Phys. Rev. Lett*. 1996, **77**, 3865-3868

[72] J. P. Perdew, K. Burke, M. Ernzerhof, *Phys. Rev. Lett*. 1997, **78**, 1396.

[73] J. VandeVondele, J. Hutter, *J. Chem. Phys*. 2003, **118**, 4365-4369.

[74] M. Krack, M. Parrinello in *High Performance Computing in Chemistry*, (Ed. J. Grotendorst), John von Neumann Institute for Computing, NIC Series, Jülich, **2005**, pp. 29 – 50.

[75] J. VandeVondele, M. Krack, F. Mohamed, M. Parrinello, T. Chassaing and J. Hutter, *Comp. Phys. Comm*. 2005, **167**, 103-128.

[76] S. Goedecker, M. Teter, J. Hutter, *Phys. Rev. B* 1996, **54**, 1703-1710.

[77] C. Hartwigsen, S. Goedecker, J. Hutter, *Phys. Rev. B* 1998, **58**, 3641-3662.

[78] M. Krack, *Theo. Chem. Account* 2005, **114**, 145-152.

[79] J. VandeVondele, J. Hutter, *J. Chem. Phys*., 2007, **127**, 114105.

[80] S. Grimme, J. Antony, S. Ehrlich, H. Krieg, *J. Chem. Phys*. 2010, **132**, 154104.

[81] M. Capdevila-Cortada, J. Ribas-Arino, J.J. Novoa, *J. Chem. Theory Comput*. 2014, **10**, 650 – 658.

[82] G. Bussi, D. Donadio, M. Parrinello, *J. Chem. Phys*. 2007, **126**, 014101.

[83] H. Jónsson, G. Mills, K. W. Jacobsen in *Classical and quantum dynamics in condensed phase simulations*, (Ed: B. J. Berne, G. Ciccotti, and D. F. Coker) World Scientific, 1998, pp. 385–404.

[84] G. Henkelman, B.P. Uberuaga, H. Jónsson, *J. Chem. Phys.*, 2000, **113**, 9901- 9904.

[85] Quantum Espresso v. 5.4.0. P. Giannozzi, O. Andreussi, T. Brumme, O. Bunau, M. Buongiorno Nardelli, M. Calandra, R. Car, C. Cavazzoni, D. Ceresoli, M. Cococcioni, N. Colonna, I. Carn- imeo, A. Dal Corso, S. de Gironcoli, P. Delugas, R. A. DiStasio Jr, A. Ferretti, A. Floris, G. Fratesi, G. Fugallo, R. Gebauer, U. Gerstmann, F. Giustino, T. Gorni, J Jia, M. Kawamura, H.-Y. Ko, A. Kokalj, E. Küçükbenli, M. Lazzeri, M. Marsili, N. Marzari, F. Mauri, N. L. Nguyen, H.-V. Nguyen, A. Otero-de-la-Roza, L. Paulatto, S. Poncé, D. Rocca, R. Sabatini, B. Santra, M. Schlipf, A. P. Seitsonen, A. Smogunov, I. Timrov, T. Thonhauser, P. Umari, N. Vast, X. Wu, S. Baroni, "Advanced capabilities for materials modelling with Quantum ESPRESSO", *J.Phys.: Condens. Matter* 2017, **29**, 465901.

[86] S. Grimme, *J. Comput. Chem*. 2006, **27**, 1787–1799.

[87] D. Vanderbilt, *Phys. Rev. B* 1990, 41.11: 7892.

[88] C. Angeli, R. Cimiraglia, S. Evangelisti, T. Leininger, J.-P. Malrieu, *J. Chem. Phys*. 2001, **114**, 10252-10264.

[89] C. Angeli, R. Cimiraglia, J.-P. Malrieu, *J. Chem. Phys*. 2002, **117**, 9138-9153.

[90] ORCA v. 4.0.1.2. F. Neese, *WIREs Comput. Mol. Sci.*, 2012, **2**, 73–78.

[91] F. Weigend and R. Ahlrichs, *Phys. Chem. Chem. Phys*., 2005, **7**, 3297-3305.

[92] K. Kitaura, K. Morokuma, *Int. J. Quantum Chem*., 1976, **10**, 325-331.

[93] P. Su, H. Li, *J. Chem. Phys.*, 2009, **131**, 014102.

[94] M.W. Schmidt, K.K. Baldridge, J.A. Boatz, S.T. Elbert, M.S. Gordon, J.H. Jensen, S. Koseki, N. Matsunaga, K.A. Nguyen, S. Su, T.L. Windus, M. Dupuis, J.A. Montgomery, *J. Comput. Chem*., 1993, **14**, 1347-1363.

[95] R. A. Kendall, T. H. Dunning Jr., and R. J. Harrison, *J. Chem. Phys.*, 1992, **96**, 6796-806.

Image for the Table of Contents Entry

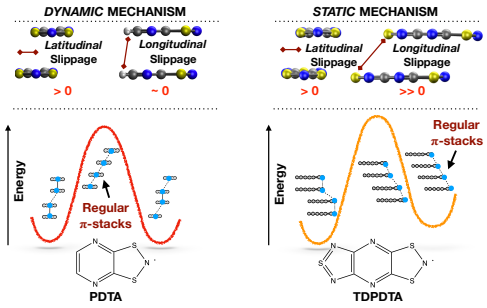

Sentence for the Table of Contents Entry

Regular π-stacks of dithiazolyl radicals can be rendered stable via two different mechanisms depending on the relative disposition of neighboring radicals